ChemCatChem

Research Article
doi.org/10.1002/cctc.202301386

Chemistry Europe
European Chemical Societies Publishing

www.chemcatchem.org

Mechanistic Pathways for the Dehydrogenation of Alkanes on Pt(111) and Ru(0001) Surfaces

Mazharul M. Islam,[a] C. Richard A. Catlow,[a] and Alberto Roldan*[a]

The dehydrogenation of alkanes is a critical process to enable olefin upcycling in a circular economy. A suitable selective catalyst is required in order to avoid demanding reaction conditions and ensure the activation of the C–H bond rather than breaking the C–C bond, which is the weaker of the two. Herein, using periodic density functional theory, we have investigated the dehydrogenation of n-pentane (as a model compound) on Pt and Ru surface catalysts. The results show that the first dehydrogenation occurs through the dissociative adsorption of the C–H bond, resulting in pentyl and H intermediates on the metal surfaces. A successive dehydrogenation creates pentene via a hydride di-σ state, leaving the abstracted hydrogen atoms on the metal surfaces. In agreement with recent experiments, Pt and Ru catalysts show a similar reactivity trend: pentane dehydrogenation yields pent-1-ene and pent-2-ene. The simulations reveal that the 1st C–H dissociation is the rate-determining step, whereas the double-bonded alkenes (pent-1-ene and pent-2-ene) are formed due to fast successive dehydrogenation processes. Pt favors the formation of pent-1-ene, whereas Ru favors the formation of pent-2-ene.

1. Introduction

Plastics have infiltrated every facet of human life. They are widely used in packaging, medical equipment, electronic devices, and many other fields because of their suitable properties, e.g., lightweight, low-cost, hydrophobicity, and durability.[1] More than 90% of plastics are petroleum-based and non-biodegradable.[2] Current plastics production and consumption patterns have dramatically increased plastic waste worldwide, and it is estimated that their manufacturing alone will consume ~20% of global petroleum by 2050.[3] The global recycling rate is low; only 16% of plastics are recycled, 14% are incinerated, and 70% are estimated to be landfilled or leaked into the environment.[4–6]

Plastics are long-lived with covalent bonds, hardly accessible for depolymerization by biological or abiotic means in landfills or natural environments.[4] In addition, plastics are formulated with other components, providing further barriers to natural decomposition at appreciable rates.[4] The current recycling approaches are mechanical-based on either post-production (primary) or post-consumption (secondary), in which plastics are transformed into new materials.[4,7] These approaches can be considered downcycling from both the material property and economic perspective and, therefore, cannot enable a fully circular plastics economy. Chemical recycling (tertiary) of plastics depolymerizes them into bulk chemicals that can either synthesize the same plastic with virgin-like material properties or convert them into another material.[8] In the present paper, we aim to investigate a catalytic polyolefin's chemical recycling route by converting alkanes into olefins, constituting a potential pathway for polyolefin upcycling.

From a chemical viewpoint, alkanes consist of nonpolar C–C and C–H bonds, composed of strongly localized electron pairs, which require severe reaction conditions for their activation.[9] Traditionally, olefin production relies on crude oil fractionation, with steam and fluid catalytic cracking.[10,11] These processes suffer from challenging drawbacks, including the use of fossil fuel, intensive energy requirements (high temperature and pressure), poor olefin selectivity and yield, and unavoidable side reactions, e.g., hydrogenolysis, cracking, isomerization, coke formation.[12–14]

The average bond energy of the C–C bond (347 kJ mol^{-1}) is smaller than that of the C–H bond (414 kJ mol^{-1}).[15] Thus, to obtain the dehydrogenation products, the C–H bond should be selectively activated in the presence of suitable catalysts. Precious metal-based homogeneous catalysts can promote mild alkane dehydrogenation reactions.[12] For instance, the combination of a titanium alkylidene catalyst and a phosphorus ylide acceptor (a hydrogen acceptor to remove two H atoms from the intermediate) converts a range of cyclic and linear alkane substrates into terminal alkenes at room temperature.[12,16] Besides, acceptor-less homogeneous alkane dehydrogenation reactions were also performed in the presence of Rh,[17,18] Ru,[19,20] Ir,[21] Pd,[22] and Os[23] based complexes. However, the main problem with using homogeneous catalysis methods is that they generate significant waste.[18] On the other hand, the dehydrogenation of light alkanes using heterogeneous catalysts based on supported metals and metal-oxides currently has a limited scope of industrial applications[24] and references there-

[a] M. M. Islam, C. R. A. Catlow, A. Roldan
Cardiff Catalysis Institute, School of Chemistry, University of Cardiff, Main Building, Park Pl, Cardiff CF10 3AT, Cardiff
E-mail: roldanmartineza@cardiff.ac.uk

Supporting information for this article is available on the WWW under https://doi.org/10.1002/cctc.202301386

in. For this reason, there is a strong need for durable and atom-efficient alkane dehydrogenation catalysts with good yield and selectivity of olefins.

Noble metal catalysts for the dehydrogenation of alkanes show significant efficiency in breaking C–H bonds.[24,25] Herein, we have studied the dehydrogenation of pentane on two noble metal catalysts, Pt and Ru, and compared their selectivity for forming olefins. Pentane was chosen as a model hydrocarbon because it does not undergo direct aromatization and is thermodynamically more stable than its longer homologs.[26] We have employed computational approaches based on the density functional theory (DFT) method to calculate dehydrogenation reaction energy profiles as a function of the catalysts' nature.

2. Models and Computational Methods

We have carried out a systematic dehydrogenation of pentane (C_5H_{12}) on the fcc Pt(111) and the hcp Ru(0001) with periodic quantum-chemical calculations using the plane-wave package VASP.[27–29] Benchmark reports have confirmed that these surfaces are the most stable for these metals.[30–32] The Density Functional Theory (DFT) calculations include the generalized gradient approximation (GGA) based revised Perdew–Burke–Ernzerhof (RPBE) exchange-correlation functional,[33,34] with long-range dispersion corrections including zero-damping function.[35,36] The core electrons for Pt, Ru, C, and H were defined by standard sets of pseudopotentials (PPs) within the projector-augmented wave (PAW) method.[37] We have used a converged plane-wave energy cutoff of 520 eV. The integration in reciprocal space was performed with a Monkhorst–Pack ***k***-points grid.[38] The grid was augmented for the bulk Pt and Ru to achieve 10^{-6} eV and 10^{-3} eV/Å for the electronic threshold and the ionic threshold convergence at 12×12×12 and 14×14×8 points, respectively. The same method, including these technical options, has been successfully employed for successive hydrogenolysis of pentane on the Ru(0001) surface.[39]

The Pt(111) and Ru(0001) slabs were modeled with increasing layers of thickness based on the optimized bulk lattice. The total energy convergence as a function of the number of layers was verified by calculating the surface energy (γ) as the difference in the total energy between the bulk and the surface per formula unit, equation 1.

$$\gamma = \frac{E_{Slab} - m\,E_{Bulk}}{2A} \tag{1}$$

E_{Slab} is the total energy of the two-dimensional slab containing m formula units of metal, E_{Bulk} is the total energy per bulk metal unit, and A is the surface area of the slab. Factor 2 in the equation accounts for the two identical surfaces, i.e., top and bottom. Surface energies for Pt(111) and Ru(0001) converged at 2.40 and 3.33 J/m^2, respectively, which are in good agreement with the previous calculated[30,40,41] and experimental values[40,42] (Table S1 in the Supporting Information). Accordingly, Pt(111) was modeled with a 4-layer slab with 4×4 supercell size where the bottom two layers were frozen at the optimized bulk lattice. For Ru(0001), a 6-layer slab with a 4×4 supercell size was employed where the bottom three layers were frozen at the optimized bulk lattice. A vacuum layer of 20 Å along the z-direction perpendicular to the surface was employed to prevent spurious interactions between the repeated slabs. The surface sizes also minimize the lateral interactions between periodic images of adsorbates. Surfaces were sampled with a converged ***k***-space Monkhorst-Pack grid of 3×3×1 points.

In order to investigate the interaction of pentane with the metal surfaces, we approached the model compound to the surface with different orientations (Figure S1). The adsorption energy (E_{Ads}) was calculated using equation 2.

$$E_{Ads} = E_{Mol+Slab} - (E_{Mol} + E_{Slab}) \tag{2}$$

The most favorable conformations have the molecule parallel to the surfaces (E_{Ads}~−0.95 eV and −0.71 eV for Pt and Ru surfaces, respectively); the perpendicular orientations have E_{Ads}~−0.26 and −0.32 eV for Pt and Ru surfaces respectively. The same conclusion was also observed for the propane adsorption on chromium-containing catalysts.[43] In the subsequent sections, we have only considered horizontal adsorptions to study the dehydrogenation process. The reaction energy (E_R) for each dehydrogenation step was calculated as the difference between the energy of the final state (E_{FS}) and the initial state (E_{IS}) with equation 3 (Table S2 in the Supporting Information).

$$E_R = E_{FS} - E_{IS} \tag{3}$$

The dehydrogenation energy variation (ΔE) along the reaction pathway was calculated with equation 4 (Table S3 in the Supporting Information).

$$\Delta E = E_{Mol-nH+Slab} - (E_{Mol} + E_{Slab}) \tag{4}$$

The transition states search along the reaction pathway was conducted using the climbing-image Nudged-Elastic-Band (cNEB) method implemented in VASP.[44] Vibrational analyses of all optimized geometries were performed to verify the local minima and saddle-point characters. Equation 5 is the difference between the transition state energy (E_{TS}) and initial state energy, which leads to the activation energy (E_A) for the forward reaction (Table S4 in the Supporting Information).

$$E_A = E_{TS} - E_{IS} \tag{5}$$

The C and H atomic charges calculated using Bader's analysis[45] are provided in Table S5.

3. Results and Discussion

The olefin formation from poorly reactive aliphatic substrates requires tandem dehydrogenation and cross metathesis (TDOCM) in which alkanes are activated through dehydrogen-

ation and functionalization or cleavage, commonly promoted by catalysts.[4,46] TDOCM processes offer selective and versatile means to depolymerize plastics under milder conditions than traditional pyrolysis or cracking methods,[46] leading to low-weight olefins and hydrogen removed from the polymer backbones due to the selective catalytic activation of the C–H and C–C bonds.[4] The pentane adsorptions on the metal surfaces are exothermic (E_{Ads}(Pt) = −0.96 eV and E_{Ads}(Ru) = −0.71 eV) and have similar molecular distortions: slight elongation of the C–H and contraction of the C–C bonds. The distance between pentane and metal surfaces (e.g., C–Pt and H–Pt are 3.11 and 1.14 Å) suggests a stabilization by long-range interactions (Figure S1). The calculated E_{Ads} on Pt are in close agreement with those obtained by Ding *et al.* (−0.84 eV).[47] The small difference in absolute value originated from different computational settings.

3.1. Reaction Energy

Pentane dehydrogenation was performed in two steps (Figure S2), each implying the C–H cleavage and hydrogen transfer to the metal surface, leading to four different reaction mechanisms: (a) dehydrogenation of the terminal (C1) and middle (C2) carbons (Figures S3 and S7); (b) dehydrogenation of the second (C2) and either the first (C1) (Figures S4 and S8) or the third (C3) carbons (Figures S5 and S9); and (c) dehydrogenation of C3 and C2, which is equivalent to C4 in the pentane molecule (Figures S6 and S10).

Once the first hydrogen is abstracted from the carbon atom, the optimized H and C distances to the surface are, respectively, about ~1.56 Å and ~2.1 Å on Pt(111) and ~1.9 Å and ~2.2 Å on Ru(0001), the former agreeing with previous reports on hydrogen adsorption.[30,48] The reaction energies of the first dehydrogenation differ slightly regarding the carbon position along the aliphatic chain (C1, C2, and C3); their values range between −0.03 to 0.18 eV on Pt(111) surface and from 0.15 to 0.35 eV on Ru(0001) surface (Table S2). For both metals, the dehydrogenation of C2 is more favorable than C1 and C3. The intermediates pass through a pentyl hydride transition state, where C_5H_{11} and H receive electrons from the surface[49] (TS2 in Figure 1). The calculated C and H atomic charges show a slightly larger charge density transfer on Ru (< 0.3 e) than on Pt (< 0.2 e) (Table S5). The formation of a bond between adsorbates and the surface is shown by the overlap of the metal d_{z^2} band with H 1s and C 2p orbitals (σ bonds) in the projected density of states (PDOS) (Figure 1).

The second dehydrogenation implies the reduction of the participating carbons from sp^3 to sp^2, forming a C=C double bond and leaving two H ad-atoms on the metal surface.[49] The reaction energies of the second dehydrogenation expand from −0.47 on Ru(0001) to 0.72 eV on Pt(111) (Table S2). For Pt, the dehydrogenation of C2–C3 is more favorable than of C1–C2, contrary to Ru. Independent of the pathway, the transition states (TS23 and TS12 in Figure 2) constitute pentene dihydride

Figure 1. Schematic representations and PDOS of C2-pentyl hydride on Pt(111) (a, b and c) and on Ru(0001) (d, e and f). The distances between metal-carbon and charges on respective atoms are provided in the inset.

Figure 2. Schematic representation and PDOS of C2–C3 pentene dihydride on Pt(111) (a, b and c) and C1–C2 pentene dihydride on Ru(0001) (d, e and f). The distances between metal-carbon and charges on respective atoms are provided in the inset.

structures,[49] leading to activation energies between 0.40–0.89 eV on Pt and 0.41–0.76 eV on Ru (Table S4). The C–C bond lies almost parallel to the metal surface with a distance of ~1.4 Å, between a single and a double bond,[50] whereas the alkyl groups point outwards, giving rise to a di-σ-mode of adsorption. Such TS structures show a transferred electron density of < 0.2 e^- on Pt and < 0.4 e^- on Ru. The most favorable pathways lead to pent-2-ene ($d_{C2=C3}$ = 1.37 Å) on Pt and to pent-1-ene ($d_{C1=C2}$ = 1.38 Å) on Ru. The TS's characteristics align with previous observations of olefin adsorptions on metal surfaces.[51,52] Note that the bonding of olefins on metal surfaces has been described as ranging from two modalities, di-σ and π bonding, of which di-σ bonding is the strongest and occurs preferentially on most clean surfaces.[52,53] Like the pentyl hydride adsorption for the first dehydrogenation, the metal-C and metal-H bonds in the TS structure are products of the metal d_{z^2} band overlap with the atomic orbitals (Figure 2). Upon overtaking the transition state for the second dehydrogenation, pentene desorbs from the metal surface (Figures S3–S10).

3.2. Reaction Profiles

The calculated energy profiles for the four main reactions are provided in Figure 3, which include the pentane adsorption, the two consecutive dehydrogenations linked by transition states, and the pentene desorption, leaving two H ad-atoms on the surface. Numeric details are given in Tables S3 and S4. The energy profiles clearly indicate the limiting rate controlled by product desorption, meaning that there is potential for consequtive dehydrogenations and possible coke formation under reaction conditions.

From the adsorbed pentane at −0.96 and −0.71 eV on Pt and Ru, with respect to the isolated molecule and pristine surfaces, the C1 dehydrogenation pathway yields a pentyl and a co-adsorbed H ad-atom releasing (E_R < 0) −0.87 and −0.52 eV upon overtaking activation energies of 0.95 and 0.87 eV, respectively. The consecutive dehydrogenation at the second carbon (C2) produces adsorbed pent-1-ene (E_R = −0.16 and −0.84 eV) through the pentene dihydride transition states (TS12; E_A = 0.88 eV and 0.41 eV). The origin of the more significant barrier for pent-1-ene formation on the Pt surface compared to the Ru surface could be associated with the larger M–C2 bond distance of the former case (d_{Pt-C1} = 2.25 Å, d_{Pt-C2} = 2.85 Å and d_{Ru-C1} = 2.21 Å, d_{Ru-C2} = 2.44 Å). Finally, the desorption of pent-1-ene from the metal surfaces requires 0.87 and 1.26 eV, respectively. These results clearly show Ru to be preferable over Pt to catalyze the formation of pent-1-ene.

An alternative reaction mechanism involves an initial dehydrogenation of C2 upon overtaking activation energies of 0.92 and 0.78 eV on Pt and Ru surfaces, respectively. In the transition states (TS2), the H and C2 interact with the metal surfaces at slightly varying distances (d_{Pt-H} = 1.61 Å, d_{Pt-C2} = 2.40 Å, and d_{Ru-H} = 1.70 Å, d_{Ru-C2} = 2.36 Å), linked to the different

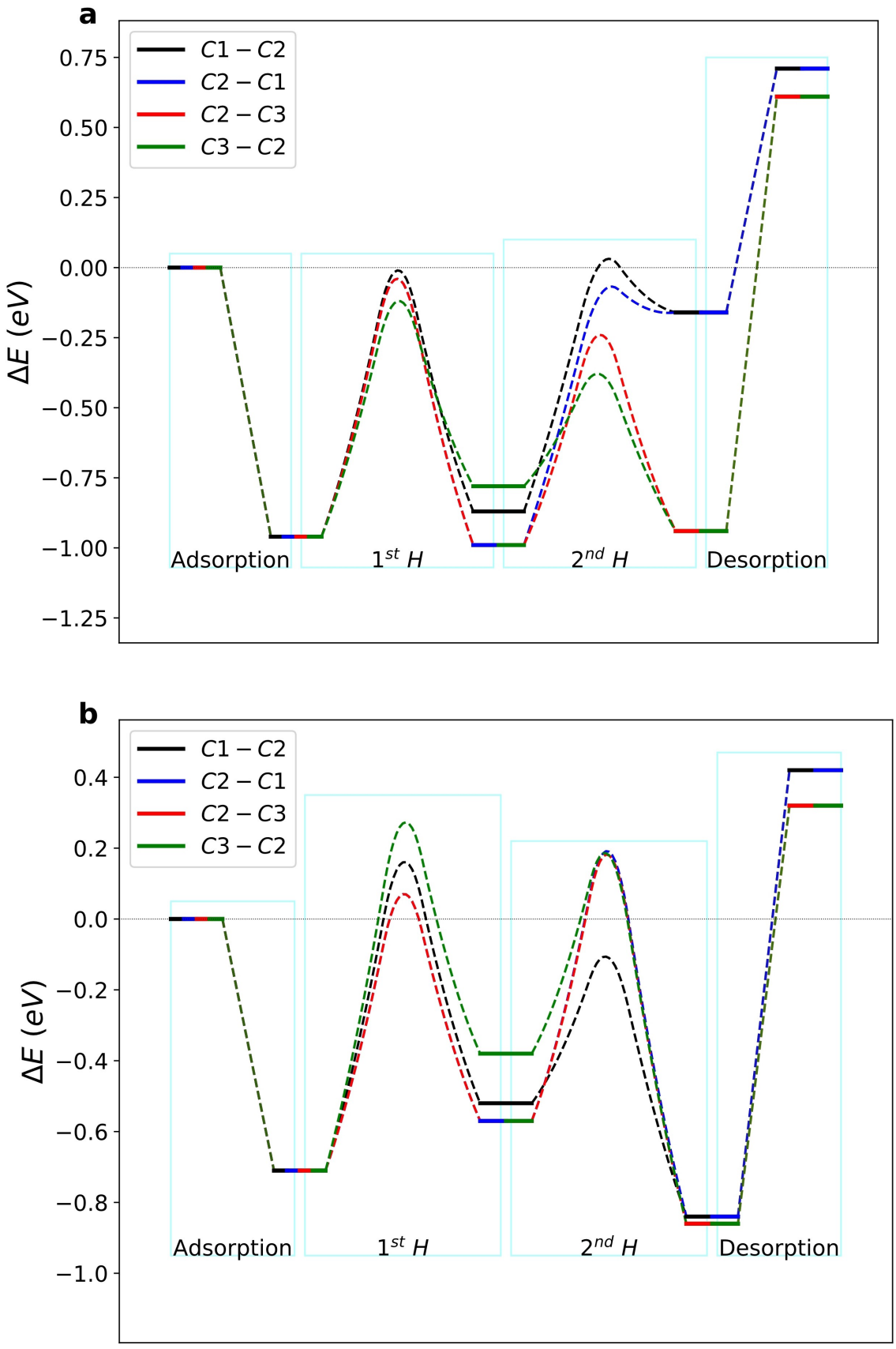

Figure 3. Energy profiles for the successive dehydrogenations of C_5H_{12} on (a) Pt(111) and (b) Ru(0001). The bell-like curves represent the activation energy (E_A) passing through the transition state energies.

atomic size of the metals. The dehydrogenation energies for forming the pentyl hydride for Pt and Ru surfaces are −0.99 eV and −0.57 eV, respectively. Then, two possible successive dehydrogenations may occur, one at the C1 site forming pent-1-ene and another at the C3 site forming pent-2-ene. The pent-1-ene formation is governed by an activation energy of 0.89 eV and 0.76 eV on Pt(111) and Ru(0001), respectively. In contrast, the pent-2-ene formation occurs by an activation energy of 0.75 eV on both surfaces. The analysis of the pentene dihydride (TS21) leading to pent-1-ene shows that, in line with their activation energies, the $d_{M\text{-}C1}$ is significantly larger for Pt (2.85 Å) than for Ru surface (2.40 Å); further analysis could determine $d_{M\text{-}C}$ as catalytic activity descriptor. The TS23 forming pent-2-ene results in the same activation energy barrier for both metals and shows that the carbon atoms (C2 and C3) interact with the metal surfaces at similar distances: $d_{M\text{-}C2}$ = 2.17–2.19 and $d_{M\text{-}C3}$ = 2.20 −2.22 Å. The competitive pathways favor pent-2-ene on Pt and pent-1-ene on Ru surfaces based on the activation and dehydrogenation energies, in agreement with recent studies where the formation of α-olefin was predominant due to the terminal regioselectivity.[54]

The last reaction mechanism explored involves the first endothermic C3 dehydrogenation (E_R = 0.18 and 0.35 eV) upon surpassing activation energies of 0.84 and 0.98 eV on the Pt(111) and Ru(0001). The consecutive dehydrogenation on the vicinal carbon (C2) has activation energies of 0.40 and 0.56 eV, respectively, leading to pent-2-ene (E_R = + 0.06 and −0.47 eV). The analysis of the transition states (TS32) shows that the M–C bond lengths are shorter on Pt(111) than on Ru(0001) ($d_{Pt\text{-}C2}$ = 2.10 and $d_{Pt\text{-}C3}$ = 2.33 Å and $d_{Ru\text{-}C2}$ = 2.18 and $d_{Ru\text{-}C2}$ = 2.48 Å) resulting in the lower activation energy for the former. By comparing the pent-2-ene formation through the routes above (C2–C3 and C3–C2), it can be stated that the C3–C2 pathway is less likely due to the significant activation barrier and poor thermodynamic drive (E_R).

The comparison of the reaction energies and activation barriers concludes that the first dehydrogenation is more likely on C2 than on C1. Despite this, the formation of pent-2-ene is preferable on Pt(111), whereas on Ru(0001), it is pent-1-ene, in line with recent observations on C_3-C_4 hydrocarbons.[43]

4. Summary and Conclusion

The dehydrogenation mechanisms of n-pentane on Pt(111) and Ru(0001) surfaces have been investigated by RPBE-D3 calculations. Upon the adsorption of pentane, the dehydrogenation occurs in two steps on the metal surfaces. The first H abstraction from terminal or middle carbons forms a pentyl hydride radical on the metal surface. The abstracted H is also attached to the metal surface. The second dehydrogenation step occurs through a di-σ-mode pentene dihydride. The analysis of PDOS shows that on both surfaces and along the reaction pathway, the M–H and M–C bonds are formed due to the overlap between metal d_{z2} and atomic orbitals. One could expect scaling relationships between the metal catalysts' electronic structure and the adsorbents' interaction. The calculated activation energies indicate that the first dehydrogenation step hinders the reaction kinetics. However, the desorption of either pent-1-ene or pent-2-ene requires more energy to overtake the transition states, especially on Pt. The pent-2-ene formation (E_A = 0.40 eV) is favorable on Pt(111), whereas on Ru(0001), pent-1-ene is preferred. Hence, the catalytic dissociation of a pentane molecule on Pt or Ru occurs via the R–CH–R′ surface intermediate (R is H or terminal C and R′ an aliphatic chain). The successive dehydrogenation on the next carbon creates a C–C double bond. The Pt and Ru catalysts show suitable capacity to convert alkanes into alkenes.

Despite the reactivity simulated, the adsorption of aliphatic chains, e.g. pentane, interact very weakly with the catalysts. Consequently, and as noted experimentally, the probability of dehydrogenating these alkanes is hampered by an equally or more feasible desorption. Furthermore, the endothermicity of the process stands out in the energy profiles when considering the pentene desorption, meaning that the dehydrogenation process requires elevated temperatures favouring the reactant desorption.

Acknowledgements

The authors acknowledge the financial support from the EPSRC-funded UK Interdisciplinary Centre for Circular Chemical Economy (NIC3E) (EP/V011863/1). Via our membership of the UK's HEC Materials Chemistry Consortium, funded by EPSRC (EP/R029431), this work used the UK Materials and Molecular Modelling Hub for computational resources, MMM Hub, which is partially funded by EPSRC (EP/T022213). We also acknowledge the Isambard 2 UK National Tier-2 HPC Service (http://gw4.ac.uk/isambard/) operated by GW4 and the UK Met Office, funded by EPSRC (EP/T022078/1), and supercomputing Wales for access to the Hawk HPC facility, part-funded by the European Regional Development Fund via the Welsh Government. All data created during this research are available from the University of Cardiff Research Portal orca websites http://doi.org/10.17035/d.2023.0291887933.

Conflict of Interests

The authors declare no conflict of interest.

Data Availability Statement

The data that support the findings of this study are openly available in C-H Bond Activation Through Catalytic Dehydrogenation Using Transition Metals at https://doi.org/10.17035/d.2023.0291887933, reference number 291887933.

Keywords: Heterogeneous Catalysis · Olefin · DFT · Plastic Upcycling · Circular Economy

[1] X. Zhao, K. Cornish, Y. Vodovotz, *Environ. Sci. Technol.* **2020**, *54*, 4712–4732.
[2] The New Plastics Economy – Rethinking The Future of Plastics (Ellen Macarthur Foundation & McKinsey & Company, **2016**).
[3] L. D. Ellis, et al., *Nat. Cat.* **2021**, *4*, 539–556.
[4] M. Hong, E. Y.-X. Chen, *Trends Chem.* **2019**, *1*, 148–151.
[5] H. Sardon, A. P. Dove, *Science* **2018**, *360(6387)*, 380–381.
[6] A. E. Schwarz, T. N. Ligthart, D. G. Bizarro, P. De Wild, B. Vreugdenhil, T. Van Harmelen, *Waste Management* **2021**, *121*, 331–342.
[7] J. M. Garcia, M. L. Robertson, *Science* **2017**, *358*, 870–872.
[8] O. O. James, S. Mandal, N. Alele, B. Chowdhury, S. Maity, *Fuel Process. Technol.* **2016**, *149*, 239–255.
[9] M. Dixit, P. Kostetskyy, G. Mpourmpakis, *ACS Catal.* **2018**, *8*, 11570–11578.
[10] A. J. L. Pombeiro, M. F. C. Guedes da Silva, *Alkane Functionalization*, John Wiley & Sons, **2018**.
[11] D. Schilter, *Nat. Rev. Chem.* **2017**, *1*, 0058.
[12] M. Abdelgaid, J. Dean, G. Mpourmpakis, *Cat. Sci. Tech.* **2020**, *10(21)*, 7194–7202.
[13] J. J. Sattler, J. Ruiz-Martinez, E. Santillan-Jimenez, B. M. Weckhuysen, *Chem. Rev.* **2014**, *114(20)*, 10613–10653.
[14] R. Georgiadis, E. R. Fisher, P. B. Armentrout, *J. Am. Chem. Soc.* **1989**, *111*, 4251–4262.
[15] D. P. Solowey, M. V. Mane, T. Kurogi, P. J. Carroll, B. C. Manor, M. H. Baik, D. J. Mindiola, *Nat. Chem.* **2017**, *9(11)*, 1126–1132.
[16] A. I. McKay, A. J. Bukvic, B. E. Tegner, A. L. Burnage, A. J. Martínez-Martínez, N. H. Rees, S. A. Macgregor, A. S. Weller, *J. Am. Chem. Soc.* **2019**, *141 (29)*, 11700–11712.
[17] A. D. Chowdhury, N. Weding, J. Julis, R. Franke, R. Jackstell, M. Beller, *Angew. Chem.* **2014**, *126(25)*, 6595–6599.
[18] B. C. Gruver, J. J. Adams, S. J. Warner, N. Arulsamy, D. M. Roddick, *Organometallics* **2011**, *30(19)*, 5133–5140.
[19] L. Huang, A. Bismuto, S. A. Rath, N. Trapp, B. Morandi, *Angew. Chem.* **2021**, *133(13)*, 7366–7372.
[20] J. Choi, A. H. R. MacArthur, M. Brookhart, A. S. Goldman, *Chem. Rev.* **2011**, *111(3)*, 1761–1779.
[21] S. Furukawa, M. Endo, T. Komatsu, *ACS Cat.* **2014**, *4(10)*, 3533–3542.
[22] B. C. Gruver, J. J. Adams, N. Arulsamy, D. M. Roddick, *Organometallics* **2013**, *32(21)*, 6468–6475.
[23] C. Li, G. Wang, *Chem. Soc. Rev.* **2021**, *50(7)*, 4359–4381.
[24] V. J. Cybulskis, B. C. Bukowski, H. T. Tseng, J. R. Gallagher, Z. Wu, E. Wegener, A. J. Kropf, B. Ravel, F. H. Ribeiro, J. Greeley, J. T. Miller, *ACS Cat.* **2017**, *7(6)*, 4173–4181.
[25] D. V. Golinskii, N. V. Vinichenko, V. V. Pashkov, I. E. Udras, O. V. Krol', V. P. Talzi, A. S. Belyi, *Kinetics and Catalysis* **2016**, *57*, 504–510.
[26] G. Kresse, J. Hafner, *Phys. Rev. B* **1993**, *47*, 558.
[27] G. Kresse, J. Hafner, *Phys. Rev. B* **1993**, *48*, 13115.
[28] G. Kresse, J. Furthmüller, J. Hafner, *Phys. Rev. B* **1994**, *50*, 13181.
[29] F. Morteo-Flores, J. Engel, A. Roldan, *Phil. Trans. Royal Soc.* A **2020**, *378*, 20200056.
[30] F. R. De Boer, W. Mattens, R. Boom, A. R. Miedema, A. K. Niessen, Transition Metal Alloys, **1988**.
[31] W. R. Tyson, W. A. Miller, *Surf. Sci.* **1977**, *62*, 267–76.
[32] B. Hammer, L. B. Hansen, J. K. Nørskov, *Phys. Rev. B.* **1999**, *59*, 7413–7421.
[33] J. P. Perdew, K. Burke, M. Ernzerhof, *Phys. Rev. Lett.* **1996**, *77*, 3865.
[34] S. Grimme, J. Antony, S. Ehrlich, S. Krieg, *J. Chem. Phys.* **2010**, *132*, 154104.
[35] S. Grimme, S. Ehrlich, L. Goerigk, *J. Comp. Chem.* **2011**, *32*, 1456.
[36] G. Kresse, J. Joubert, *Phys. Rev. B* **1999**, *59*, 1758–1775.
[37] H. J. Monkhorst, J. D. Pack, *Phys. Rev.* **1976**, *13*, 5188.
[38] A. Tomer, M. M. Islam, M. Bahri, D. R. Inns, T. D. Manning, J. B. Claridge, N. D. Browning, C. R. A. Catlow, A. Roldan, A. P. Katsoulidis, M. J. Rosseinsky, *Appl. Cat. A* **2023**, *666*, 119431. (https://doi.org/10.1016/j.apcata.2023.119431).
[39] L. Vitos, A. Ruban, H. L. Skriver, J. Kollar, *Surf. Sci.* **1998**, *411(1-2)*, 186–202.
[40] M. Methfessel, D. Hennig, M. Scheffler, *Phys. Rev. B* **1992**, *46(8)*, 4816.
[41] W. R Tyson, W. A. Miller, *Surf. Sci.* **1977**, *62(1)*, 267–76.
[42] Y. Du, Y. Wang, C. Zhang, R. Li, B. Wang, S. Li, C. Yang, *Fuel* **2022**, *320*, 123893.
[43] H. Jónsson, G. Mills, K. W. Jacobsen, in *Classical and Quantum Dynamics in Condensed Phase Simulations* (Eds.: B. J. Berne, G. Ciccotti, D. F. Coker), World Scientific, Singapore, **1998**, 385.
[44] R. F. W. Bader, W. H. Henneker, P. E. Cade, *J. Chem. Phys.* **1967**, *46(9)*, 3341–3363.
[45] L. D. Ellis, S. V. Orski, G. A. Kenlaw, A. G. Norman, K. L. Beers, Y. Román-Leshkov, G. T. Beckham, *ACS Sust. Chem. Eng.* **2021**, *9(2)*, 623–628.
[46] X. Ding, H. Zhu, H. Ren, D. Liu, Z. Yu, N. Shi, W. Guo, *Phys. Chem. Chem. Phys.* **2020**, *22(38)*, 21835–21843.
[47] P. Ferrin, S. Kandoi, A. U. Nilekar, M. Mavrikakis, *Surf. Sci.* **2012**, *606*, 679–689.
[48] M. J. Burk, R. H. Crabtree, *J. Am. Chem. Soc.* **1987**, *109(26)*, 8025–8032.
[49] L. Pauling, L. O. Brockway, *J. Am. Chem. Soc.* **1937**, *59(7)*, 1223–1236.
[50] J. Zhu, M. L. Yang, Y. Yu, Y. A. Zhu, Z. J. Sui, X. G. Zhou, A. Holmen, D. Chen, *ACS Cat.* **2015**, *5(11)*, 6310–6319.
[51] F. Zaera, *Phys. Chem. Chem. Phys.* **2013**, *15(29)*, 11988–12003.
[52] F. Zaera, *Langmuir* **1996**, *12(1)*, 88–94.
[53] S. Biswas, M. J. Blessent, B. M. Gordon, T. Zhou, S. Malakar, D. Y. Wang, K. Krogh-Jespersen, A. S. Goldman, *ACS Cat.* **2021**, *11(19)*, 12038–12051.
[54] X. Chen, M. Peng, X. Cai, Y. Chen, Z. Jia, Y. Deng, B. Mei, Z. Jiang, D. Xiao, X. Wen, N. Wang, *Nat. Comm.* **2021**, *12(1)*, 2664.

Manuscript received: October 30, 2023
Revised manuscript received: February 8, 2024
Accepted manuscript online: February 9, 2024
Version of record online: ■■, ■■

RESEARCH ARTICLE

*M. M. Islam, C. R. A. Catlow, A. Roldan**

There is a growing awareness of the negative effects of plastic waste on the environment, leading to a shift towards a more sustainable "circular plastic economy." However, current recycling methods are limited by being primarily mechanical based, hindering the full realization of a truly circular plastics economy. In this paper, we explore a promising catalytic chemical recycling process that can convert polyolefins into olefins, offering new pathways for upcycling and contributing to the goal of a circular plastics economy.